536106

ATOMIC DATA AND SPECTRAL LINE INTENSITIES FOR Ne III

A. K. Bhatia[1], R. J. Thomas[1], and E. Landi[2]
[1]NASA/Goddard Space Flight Center
Greenbelt, Maryland 20771 USA

[2]Naval Research Laboratory
Washington DC 20375

ABSTRACT

Electron impact collision strengths, energy levels, oscillator strengths and spontaneous radiative decay rates are calculated for Ne III. The configurations used are $2s^22p^4$, $2s2p^5$, $2s^22p^33s$, and $2s^23p^33d$ giving rise to 57 fine-structure levels in intermediate coupling. Collision strengths are calculated at five incident energies, 5, 10, 15, 20, and 25 Ry. Excitation rate coefficients are calculated by assuming a Maxwellian electron velocity distribution at an electron temperature of $\log T_e(K)=5.0$, corresponding to maximum abundance of Ne III. Using the excitation rate coefficients and the radiative transition rates, statistical equilibrium equations for level populations are solved at electron densities covering the range of 10^8-10^{14} cm^{-3}. Relative spectral line intensities are calculated. Proton excitation rates between the lowest three levels have been included in the statistical equilibrium equations. The predicted Ne III line intensities are compared with SERTS rocket measurements of a solar active region and of a laboratory EUV light source.

CONTENTS

INTRODUCTION

Electron-impact-induced spectra of Ne are of interest in technological and astrophysical applications. The knowledge of electron-impact excitation cross sections are important for the technological development of discharge systems such as Ne-discharge light sources, the He-Ne laser, and the Ne-Xe-NF$_2$ laser where Neon plays an important role (Phillips et al. [1]).

Early laboratory measurements of Ne III have been summarized by Persson et al. [2]. They report a number of experiments on the observations of Ne III lines and a very thorough analysis of the Ne III spectrum between 130 to 12000 Å emitted by a hollow-cathode and θ-pinch discharge. These authors report a very complete list of laboratory energy levels, obtained after the identification of some 750 transitions and intensities visually estimated from the photographic density of the lines. However, such measurements are too rough to be suitable for comparison with theoretical calculations or to be of use for diagnostic purposes. More recently, James et al. [3] have measured electron-impact excitation cross section for transitions in the far ultraviolet wavelength range between 1200 to 2700 Å using an electron-ion impact collision chamber. Daw et al. [4] have measured the transition rates for the two Ne III forbidden transitions $^1S_0 \rightarrow {}^3P_1$ and $^1S_0 \rightarrow {}^1D_2$ within the ground configuration.

Neon plays an important role in a variety of astrophysical phenomena, since it is the most abundant rare gas in the universe after helium. Forbidden Ne III lines have been observed in a variety of astrophysical plasmas. The lines at 36μm and 3869 Å, due to forbidden $^3P_0 \rightarrow {}^3P_1$ and $^1D_2 \rightarrow {}^3P_2$ transitions within the ground configuration, have been observed in H II regions by a number of authors (Simpson et al. [5], Rubin et al. [6], Baldwin et al. [7], and Colgan et al. [8]); their apparent excess of observed intensity has been useful to model the photoionizing flux coming from nearby O stars (Sellmaier et al. [9]) and to investigate its effects on the ionization structure of such astrophysical objects. The 3869 Å line has also been used to measure Neon abundance, and the ratio of this line to a forbidden O II line has been used as a tool to investigate the presence of neutral and ionized helium in H II regions (Ali et al. [10]), a quantity that is important for testing models of galactic and primordial nucleosynthesis.

The Ne III 3869 Å line is also present in Ne-rich filaments in Supernova Cas A remnants (Minkowski [11] and Fesen [12]) and can be used to investigate the neon abundance of the remnant and its spatial distribution. Zheng et al. [13] have identified the 3869 Å line also in three low-redshift quasars.

The Ne III lines have also been observed in planetary nebulae: Clegg et al. [14] report the 3869 Å and several $3s$-$3p$ transitions in the planetary nebula NGC 3918. Shure et al. [15] show that the Ne III lines at 3869 Å, 36μm, and 15.6μm [$2p^4$ ($^3P_1 \rightarrow {}^3P_2$)] can be used to determine the physical properties in the NGC 6543 nebula: the 3869Å/36μm ratio can help in temperature diagnostics, and the 15.6μm/36μm is a good electron density indicator in nebular conditions. Abundance determination in Nova V351 Puppis 1991 has been carried out by Saizar [16]; the Ne III lines in Nova Cygni 1992 have been observed by Shore et al. [17] and Barger et al. [18].

The allowed line at 489.50 Å due to the transition $2s2p^5\ {}^3P_2 \rightarrow 2s^22p^4\ {}^3P_2$ has been identified in the solar spectrum by Vernazza and Reeves [19] using *Skylab* observations. This line has been detected in a variety of different physical conditions, from coronal hole to active regions. However, the presence of this line in active regions and in off-disk spectra seems to suggest that it is probably blended with another line emitted by a hotter ion.

Other Ne III lines in the solar EUV spectrum have been reported by Thomas and Neupert [20] based on observations from the Solar EUV Rocket Telescope and Spectrograph (SERTS) instrument. These include two lines arising from transitions of $3p^33s \rightarrow 2p^4$ (283.2 Å, a self blend of $^3D_2 \rightarrow {}^3P_2$ with $^3D_3 \rightarrow {}^3P_2$, and 322.7 Å, which involves the transition $^5S_2 \rightarrow {}^3P_2$), and two lines arising from transitions of $2p^33s \rightarrow 2p^4$ (379.31 Å $^1P_1 \rightarrow {}^1D_2$ and 427.84 Å $^1P_1 \rightarrow {}^1S_0$). In a comparison of that spectrum with the CHIANTI database, Young, Landi and Thomas [21] noted that the first two of these identifications could not be confirmed because of a lack of atomic data for the Ne III $2p^33s$ configuration. They further claimed that the strength of the observed 427.84 Å line suggests that it may be due to some other ion.

Clearly accurate atomic data for Ne III are critical for the proper identification of various spectral lines and to correctly infer properties of solar and astrophysical plasmas. The calculated data presented here will be useful for the interpretation of many current and future observations.

In order to interpret data from space missions, atomic data such as energy levels, oscillator strengths, radiative transition rates, and collision strengths are required. Distorted wave calculations have been carried out for a number of ions such as Fe X [22], Fe XI [23], Fe XVII [24] and Fe XXI [25] in the past.

In this paper we carry out a distorted wave calculation for Ne III in the same way as for the Fe ions mentioned above. Since coupling between various channels is not included in the distorted wave approximation, the present calculation does not include resonances which could be important for forbidden transitions but usually not for dipole-allowed transitions for which most of the contribution to collision strengths comes from a very large number of incident partial waves.

We present energy levels, oscillator strengths, radiative transition rates, and collision strengths for Ne III for 57 fine-structure levels obtained by using the configurations $2s^22p^4$, $2s2p^5$, $2s^22p^33s$, and $2s^22p^33d$ above the He-like core $1s^2$. These configurations give rise to 57 fine-structure levels in intermediate coupling.

We solve the statistical equilibrium equations for level populations at $\log T_e(K)=5.0$ where T_e is the temperature of maximum abundance of Ne III. For the known radiative transition rates the intensities of strong spectral lines can be calculated.

Atomic Data

The atomic data have been calculated using computer programs originally developed at University College London. These programs have been updated over the years. The energy levels, oscillator strengths, and radiative transition rates have been calculated by using the Superstructure program described by Eissner et al. [26]. The wavefunctions are of configuration interaction type and each configuration is expanded in terms of Slater orbitals. As indicated above, the configurations included are $2s^22p^4$, $2s2p^5$, $2s^22p^33s$, and $2s^22p^33d$. The radial functions are calculated in a scaled Thomas-Fermi-Amaldi potential. The potential depends upon parameters λ_l which are determined variationally by optimizing the weighted sum of the term energies. They are found to be $\lambda_0 = 1.2467$, $\lambda_1 = 1.1617$, and $\lambda_2 = 1.0663$. The relativistic corrections are included by using Breit-Pauli Hamiltonian as a perturbation to the nonrelativistic Hamiltonian. Energy levels, oscillator strengths, and radiative transition rates are calculated in intermediate coupling. The calculated energies for Ne III are listed in Table I. We use the calculated energy values to compute oscillator strengths and transition rates. The calculated energies are compared with the experimental energies compiled by Fuhr et al. [27].

The scattering problem is carried out in the distorted wave approximation using programs described by Eissner and Seaton [28] and Eissner [29]. The reactance matrices at incident energies 5, 15, 26, 35, and 45 Ry are calculated in LS coupling. The collision strengths in intermediate coupling are calculated using these reactance matrices and the term-coupling coefficients obtained from structure calculations in the program JAJOM developed by Saraph [30] and modified recently by Saraph and Eissner [31]. The distorted wave calculations are carried out including intermediate angular momentum states L^T up to 33. The angular momentum L^T of the intermediate state is defined as

$$\vec{L^T} = \vec{l_i} + \vec{l_t} \tag{1}$$

where $\vec{l_i}$ is the angular momentum of the incident electron and $\vec{l_t}$ is the angular momentum of the target level. There is a considerable contribution to collision strengths from higher partial waves l_i, and we have added Coulomb-Bethe contributions for $l_i > 29$ to the dipole-allowed collision strengths. This contribution is calculated in the Coulomb-Bethe approximation using the program of Burgess and Sheorey [32]. The contributions from the higher partial waves to the non-dipole-allowed transitions have been added using the geometric progression. These additional contributions are referred to as top-up and this feature has recently been added to the program JAJOM [31].

The convergence of the collision strengths with respect to L^T has been demonstrated in most of the previous publications when the maximum L^T was 21. In the present case L^T is 33 and we expect all collision strengths to have converged. The Ne III collision strengths Ω_{ij}, the transition rates A_{ji}, and $g_i f_{ij}$, the absorption oscillator strengths multiplied by the statistical weight g_i of the lower level i are given in Table II. The latter parameters are related by the expression

$$A_{ji} = \frac{6.670 \times 10^{15} g_i f_{ij}}{\lambda^2(\AA) g_j} \tag{2}$$

Line Emissivity

The number of photons observed in optically thin spectral line $j \to i$ is given by

$$I_{ji} = \frac{1}{4\pi} \int_h N_j(X^{+m}) A_{ji} dh \qquad ph\ cm^{-2}\ s^{-1}\ sr^{-1} \tag{3}$$

If the *Contribution Function* $G_{ij}(T, N_e)$ of the line is defined as

$$G(T, \lambda_{ij}) = \frac{N_j(X^{+m})}{N(X^{+m})} \frac{N(X^{+m})}{N(X)} \frac{N(X)}{N(H)} \frac{N(H)}{N_e} \frac{A_{ji}}{N_e} \tag{4}$$

where

1. – $\frac{N_j(X^{+m})}{N(X^{+m})}$ is the relative upper level population;
2. – $\frac{N(X^{+m})}{N(X)}$ is the relative abundance of the ion X^{+m} (*ion fraction*); this quantity is taken from the literature under the assumption of ionization equilibrium;
3. – $\frac{N(X)}{N(H)}$ is the abundance of the element X relative to hydrogen;
4. – $\frac{N(H)}{N_e}$ is the hydrogen abundance relative to the electron density (≈ 0.8 for fully ionized plasmas);
5. – A_{ji} is the Einstein coefficient for spontaneous emission.

and the *Differential Emission Measure* (DEM) is introduced as

$$\varphi(T) = N_e^2 \frac{dh}{dT} \tag{5}$$

the number of photons emitted in a spectral line may be expressed as

$$I_{ji} = \frac{1}{4\pi} \times \int_T G(T, \lambda_{i,j}) \varphi(T) dT \tag{6}$$

In the present work, we are interested in evaluating the $G_{ij}(T, N_e)$ function for all the Ne III lines.

The relative population $\frac{N_j(X^{+m})}{N(X^{+m})}$ must be calculated by solving the statistical equilibrium equations for a number of low lying levels and including all the important collisional and radiative excitation and de-excitation mechanisms:

$$N_i(N_e\Sigma_{j<i}C^{e}_{ji} + N_p\Sigma_{j<i}C^{p}_{ji} + N_e\Sigma_{j>i}C^{ed}_{ji} + N_p\Sigma_{j>i}C^{pd}_{ji} + \Sigma_{i>j}R_{ji} + \Sigma_{i<j}A_{ji}) =$$
$$\Sigma_{i<j}N_i(N_eC^{e}_{ij} + N_pC^{p}_{ij}) + \Sigma_{i>j}N_i(N_eC^{ed}_{ij} + N_pC^{pd}_{ij}) + \Sigma_{i>j}N_iA_{ij} + \Sigma_{i<j}N_iR_{ij} \qquad (7)$$

with C^{e}_{ij} and C^{p}_{ij} the electron and proton collisional excitation rate coefficients (cm^3 sec^{-1}) from the level i to the level j, R_{ji} the stimulated absorption rate coefficient (sec^{-1}) and A_{ji} the spontaneous radiative transition rate (sec^{-1}). C^{e} and C^{pd} are the electron and proton dexcitation rate coefficients. In typical astrophysical or laboratory conditions it is possible to neglect the stimulated absorption and emission mechanisms. However, since Ne III is formed at very high temperatures, proton rates may give a significant contribution to the population of excited levels, and so they cannot be neglected.

Collisional Data Fitting Technique

The electron excitation coefficient C^{e}_{ij} is given by

$$C^{e}_{ij} = \frac{8.63\times10^{-6}}{T_e^{1/2}}\frac{\Upsilon_{ij}(T_e)}{g_i}\,exp\left(-\frac{E_{ij}}{kT_e}\right) \qquad (8)$$

where g_i is the statistical weight of level i; E_{ij} is the energy difference between levels i and j; k is the Boltzmann constant and $\Upsilon_{i,j}$ is the thermally-averaged collision strength:

$$\Upsilon_{ij}(T_e) = \int_0^{\infty}\Omega_{i,j}\,exp\left(-\frac{E_j}{kT_e}\right)d\left(\frac{E_j}{kT_e}\right) \qquad (9)$$

where E$_j$ is the energy of the scattered electron relative to the final energy state of the ion, and Ω_{ij} is the collision strength for the transition i to j.

In order to carry out the integration in Equation (9), it is necessary to know the collision strength Ω across the whole energy range, from threshold to infinity. However, theoretical calculations only provide the collision strength for a limited number of energy values (i.e., in the case of the present Ne III calculation, only five energy values are provided), so that some interpolation/extrapolation technique is required in order to properly take into account the energy dependence of the collision strength.

In the present work we have adopted the method described by Burgess and Tully [33] to extrapolate the collision strengths to the high- and low-energy limit. This method consists of scaling both the electron energy and the collision strengths according to the transition types: allowed, forbidden and intercombination transitions. Different scaling laws have been developed in order to better reproduce the behavior of the collision strengths according to each type of transition. The scaling laws are:

$$E_{scal} = 1 - \frac{\ln C_\Omega}{\ln\left(\frac{E}{E_{ij}} + C_\Omega\right)} \qquad \Omega_{scal} = \frac{\Omega}{\ln\left(\frac{E}{E_{ij}} + e\right)} \qquad (10)$$

for the allowed transitions,

$$E_{scal} = \frac{\frac{E}{E_{ij}}}{\frac{E}{E_{ij}} + C_\Omega} \qquad \Omega_{scal} = \Omega \qquad (11)$$

for the forbidden transitions, and

$$E_{scal} = \frac{\frac{E}{E_{ij}}}{\frac{E}{E_{ij}} + C_{\Omega}} \qquad \Omega_{scal} = \left(\frac{E}{E_{ij}} + 1\right)^2 \Omega \tag{12}$$

for the intercombination transitions. The constant C_{Ω} is chosen to optimize the fit of the calculated data.

In the case of the allowed transitions, the Ω value at $E \to \infty$ ($E_{scal} = 1$) is set to be the transition's oscillator strengths, according to the Coulomb-Bethe approximation. The collision strengths are then interpolated for intermediate values of E_{scal}, and extrapolated to $E_{scal} = 0$ and $E_{scal} = 1$ (corresponding to E=0 and E$\to \infty$): the interpolated/extrapolated values are used to calculate the effective collision strength according to Equation (9). This scaling has two main advantages:

1. It allows one to calculate the effective collision strengths more accurately by better sampling the energy dependence of the collision strength;
2. It allows one to take into account the high-energy behavior of the collision strength.

The high energy behavior of the collision strength is of particular importance for the allowed transitions, as its contribution to the calculation of the effective collision strength can be very important. The use of the Coulomb-Bethe approximation allows us to use the oscillator strength of the transition both as a high-energy point for the interpolation and integration procedures, and to have an independent check on the quality of the calculation of the collision strength itself.

Results

The atomic data and transition probabilities calculated in the present work and given in Table II have been used to solve the statistical equlibrium equations (7). The proton excitation rates given by Ryans et al. [34] have been also used. The proton rate coefficients at log T_e=5.0 are 9.56×10^{-10} (1$\to$2), 2.97×10^{-10} (1$\to$3) and 8.03×10^{-11} (2$\to$3) cm^3 s^{-1}. The ion fraction given by Mazzotta et al. [35] is 0.77 and the element abundance relative to hydrogen given by Feldman [36] is 1.20×10^{-4}.

Tables IIIA and IIIB list the fractional level populations $\frac{N_j(X^{+m})}{N(X^{+m})}$ for all the levels in the Ne III atomic model, calculated without and with the proton excitation rates, respectively, at log N_e=8 to 14. The differences between the two computations are significant, but limited to a maximum of 15 % in the worst cases, and that too only in the ground ^{3}P levels. The only levels having a significant population belong to the ground configuration. However, at high density, a few more metastable levels reach a significant population, these being the levels $^1D_2$ and $^1S_0$ in the ground configuration and the $2s^22p^33s$ $^5S_2$ level, whose radiative decay is due only to intercombination or forbidden transitions with small Einstein coefficients A_{ji}.

Tables IVA and IVB list the relative line emissivities in photon units (the absolute emissivities can be obtained by multiplying the relative emissivities by the appropriate factors given earlier) for the strongest lines emitted by Ne III, calculated again without and with proton rates, respectively. The strongest Ne III transitions are found in the Extreme Ultraviolet (EUV) spectral range, at around 490 Å, these being the optically allowed $n = 2 \to n = 2$ transitions. There are a number of optically allowed transitions between $n = 3$ and $n = 2$, giving lines in the 210 to 310 Å wavelength range. The forbidden lines fall between the ultraviolet and infrared ranges.

Diagnostic potential

Only the forbidden lines arising from the ground configuration levels show a marked density sensitivity in the range $10^8 - 10^{10}$ cm^{-3}, which is typical of the solar and stellar coronae, although their predicted intensity decreases as density increases, making them difficult to observe. All the other lines are predicted to be fairly density insensitive in this density range, and so their density diagnostic potential is low. However, this property makes Ne III lines very useful for Differential Emission Measure (DEM) and Emission Measure (EM) diagnostics (see e.g., Mason and Monsignori Fossi [37]).

At lower densities a few of these lines can become useful density diagnostics, although processes other than collisional excitation, de-excitation and radiative decay can play an important role in lower density plasmas, such as those found in supernova remnants, active galactic nuclei and H II regions. These processes (photoexcitation, photoionization) can substantially alter the results reported in Tables IVA and IVB, so that the present predictions are not adequate to assess the Ne III diagnostic potential in such plasmas.

The energy difference between the $n = 2$ and $n = 3$ levels is large enough to allow a strong relative temperature sensitivity in ratios involving one $n = 2$ and one $n = 3$ lines, so that such line pairs, if observed simultaneously, can be a powerful tool for temperature diagnostics.

Comparison with SERTS Measurements

Thomas and Neupert [20] reported the wavelengths and absolute intensities of more than 200 EUV emission lines from a single solar active region observed during the SERTS rocket flight of 1989 May 5. Subsequent analyses of this full spectrum (e.g., by Brickhouse, Raymond, and Smith [38]) show that the density of the emitting plasma was on the order of 10^{10} cm^{-3} at temperatures near that of Ne III formation. The SERTS-89 intensities for the four solar lines originally identified with Ne III are reproduced here in Table A.

The observed 322Å/283Å intensity ratio of 0.74±0.45 agrees within measurement uncertainties with the predicted value of 0.91 (all ratios in this section are given in energy units). However, the measured 427Å/379Å ratio of 0.51±0.28 is significantly higher than the predicted value of 0.076, which should be particularly accurate since it is a branching ratio of transition rates and therefore strictly insensitive to variations in the emitting plasma. Thus our result confirms the suggestion by Young, Landi, and Thomas [21] that the observed solar feature at 427.8 Å is due to some ion other than Ne III. In addition, the observed intensity ratios 379Å/283Å and 379Å/322Å of 0.28±0.15 and 0.37±0.18 are both nearly a factor of 30 smaller than the predicted values of 9.25 and 10.28, respectively. This latter discrepancy needs to be checked by future observations and theoretical calculations.

Before and after each SERTS flight, the instrument is thoroughly tested in the laboratory to characterize its wavelength scale and EUV spectral response. These tests use a hollow cathode light source containing Neon gas excited by an electrical discharge, nominally at 1750 Volt and 700 milliamp (Swartz et al. [39]). Parts of one such test spectrum with several lines from Ne III are shown in Figure 1. These data were recorded on film, microdensitometered, and converted to intensity units through a standard D-logE analysis, but have not otherwise been radiometrically calibrated. Since the instrument response changes only slowly with wavelength, they can be used to indicate relative line strengths over the narrow wavelength intervals shown. The Ne III density in the laboratory source is not known, so we compare these measurements in Table B with the present results at the extremes of the calculation range.

For all of the line ratios that are relatively insensitive to density, the measurements agree very well with their corresponding calculated values. The other two, involving 282.49 and 308.56 Å, are factors of 4.3 and 2.2 larger than theoretical values at densities of 10^{14}, perhaps indicating that the plasma in the laboratory source lamp is at an even higher density.

Brosius, Thomas, and Davila [40] used these SERTS laboratory measurements to derive extremely precise wavelengths for the full set of lines that could be detected between 260 - 450 Å, as listed in Table 2 of their paper. The values for all eight of the Ne III features are reproduced here in Table C.

This data set has been made available in the CHIANTI database [42]. We hope the data presented in this paper will be useful to analyze observations of Ne III lines from the Sun and other astrophysical objects.

Acknowledgment

This work was supported by NASA grant from the Applied Information Systems Research Program under Contract W19.539. The work of Enrico Landi is supported by the Office of Naval Research. Calculations were carried out using Cray Y-MP computer of the NASA Center for Computation Science.

References

1. M. H. Phillips, L. W. Anderson, C. C. Lin, 1985, Phys. Rev. A, **32**, 2117 (1985)
2. W. Persson, C.-G. Wahlström, L. Jönsson, H. O. Di Rocco, Phys. Rev. A, **43**, 4791 (1991)
3. G. K. James, I. Kanik, and J. M. Ajello, Astrophys. J. **455**, 769 (1995)
4. A. Daw, W. H. Perkinson, and P. L. Smith, Astrophys. J. **533**, L179 (2000)
5. J. P. Simpson, S. W. J. Colgan, R. H. Rubin, E. F. Erickson, and M. R. Haas, Astrophys. J. **444**, 721 (1995)
6. R. H. Rubin, J. P. Simpson, M. R. Haas, E. F. Erickson, Astrophys. J. **374**, 564 (1991)
7. J. A. Baldwin, G. J. Ferland, P. G. Martin, M. R. Corbin, S. A. Cota, B. M. Peterson, and A. Slettebak, Astrophys. J. **374**, 580 (1991)
8. S. W. J. Colgan, M. R. Haas, E. F. Erickson, R. H. Rubin, J. P. Simpson, and R. W. Russell, Astrophys. J. **413**, 237 (1993)
9. F. H. Sellmaier, T. Yamamoto, A. W. A. Pauldrach, and R. H. Rubin, Astron. Astrophys. **395**, L37 (1996)
10. B. Ali, R. D. Blum, T. E. Bumgardner, S. R. Cranmer, G. J. Ferland, R. I. Haefner, and G. P. Tiede, Publ. Astr. Soc. Pac., **103**, 1182 (1991)
11. R. Minkowski, *RadioAstronomy*, IAU Symp. 4, eds. H.C. Van de Hulst, (Cambridge University, Cambridge), p.107 (1957)
12. R. A. Fesen, Astr. J., **99**, 1904 (1990)
13. W. Zheng, E. M. Burbridge, H. E. Smith, Publ. Astr. Soc. Pac., **102**, 497 (1990)
14. R. E. S. Clegg, P. J. Storey, and J. P. Harrington, MNRAS, **221**, 61 (1986)
15. M. A. Shure, J. R. Houck, G. E. Gull, and T. Herter, Astrophys. J. **281**, L29 (1984)
16. P. Saizar, I. Pachoulakis, S. N. Shore, S. Starrfield, S., R. E. Williams, E. Rothschild, and G. Sonneborn, MNRAS, **279**, 280 (1996)
17. S. N. Shore, G. Sonnenborn, S. Starrfield, and R. Riestra-Gonzalez, and T. B. Ake, T.B. Astr. J., **106**, 2408 (1993)
18. A. J. Barger, J. S. Gallagher, K .S. Bjorkman, K. A. Johansen, and K. H. Nordsieck, Astrophys. J. **419**, 85 (1993)
19. J. E. Vernazza, and E. M. Reeves, Astrophys. J. Suppl. **37**, 485 (1978)
20. R.J. Thomas and W.M. Neupert, Astrophys. J. Suppl. **91**, 461 (1994)
21. P.R. Young, E. Landi, and R.J. Thomas, Astron. and Astrophys. **329**, 291 (1998)
22. A. K. Bhatia and G. A. Doschek, ATOMIC DATA AND NUCLEAR DATA TABLES **60**, 97 (1995)
23. A. K. Bhatia and G. A. Doschek, ATOMIC DATA AND NUCLEAR DATA TABLES **64**, 183 (1996)
24. A. K. Bhatia and G. A. Doschek, ATOMIC DATA AND NUCLEAR DATA TABLES **52**, 1 (1992)
25. K. J. H. Phillips, A. K. Bhatia, H. E. Mason, and D. M. Zarro, Astrophys. J. **466**, 549 (1996)
26. W. Eissner, M. Jones, and H. Nussbaumer, Comput. Phys. Commun. **8**, 270 (1972)

27. J. R. Fuhr, D. E. Kelleher, W. C. Martin, A. Musgrove, J. Sugar, W. L. Wiese, G. R. Dalton, R. A. Dragoset, P. J. Mohr, K. Olsen, J. Reader, E. B. Saloman, C. J. Sansonetti, and G. Wiersma, "NIST Atomic Spectra Database" ver. 2.0 March 1999. NIST Physical Reference Data.

28. W. Eissner and M. J. Seaton, J. Phys. B **5**, 2187 (1979)

29. W. Eissner, Comput. Phys. Commun. **114**, 295 (1998)

30. H. E. Saraph, Comput. Phys. Commun. **15**, 247 (1978)

31. H. E. Saraph and W. Eissner, Comput. Phys. Commun. (to be published)

32. A. Burgess and V. B. Sheorey, J. Phys. B **7**, 2403 (1974)

33. A. Burgess, J. A. Tully, Astron. and Astrophys. **254**, 436 (1992)

34. R. S. I. Ryans, F. P. Keenan, R. H. G. Reid, ATOMIC DATA AND NUCLEAR DATA TABLES, (in preparation), (2001)

35. P. Mazzotta, G. Mazzitelli, S. Colafrancesco, and N. Vittorio, Astron. and Astrophys. **133**, 403 (1998)

36. U. Feldman, Phys. Scr.**46**, 202 (1992)

37. H. E. Mason and B. C. Monsignori Fossi, Astron. Astroph. Review 6, 123 (1994)

38. N.S. Brickhouse, J.C. Raymond, and B.W. Smith, Astrophys. J. Suppl. **97**, 551, (1995)

39. M. Swartz, C.E. Condor, J.M. Davila, J.P. Haas, S.D. Jordan, D.L. Linard, J.J. Miko, I.C. Nash, J. Novello, L.J. Payne, T.B. Plummer, R.J. Thomas, L.A. White, J.W. Brosius, and W.T. Thompson, NASA Technical Publication, NASA/TP-1999-208640, (1999)

40. J.W. Brosius, R.J. Thomas, and J.M. Davila, Astrophys. J. **526**, 494, (1999)

41. R.L. Kelly, J. Phys. Chem. Ref. Data, 16, Suppl., **1**, 1371, (1987)

42. K. P. Dere, H. E. Mason, B. C. Monsignori Fossi, and P. R. Young, Astron.Astroph. Suppl. **125**, 149 (1997)

Table I. Calculated Energy Levels for Ne III

Key	A number assigned to each level
Configuration	The configuration with $1s^2 2s^2 2p^4$ truncated
Level	The term designation of the level within the configuration
Energy	calculated level energies in units of cm^{-1}

Table II. Ne III Oscillator Stengths, Radiative Decay Rates, and Collision Strengths

Lower and Upper Level	The lower and upper levels, where the numbers refer to the Key listed in Table I
Oscillator Strength	gf, the (dimensionless) product of the statistical weight g of the lower level and the absorption oscillator strength f
Radiative Decay Rate	The spontaneous radiative decay rate A_{ji} in units of s^{-1}
Collision Strength	The dimensionless electron impact collision strength Ω at the energy (in units of Ry) given in the table heading

Table IIIA. Ne III Fractional Level Populations: Without Proton Excitation
Table IIIB. Ne III Fractional Level Populations: With Proton Excitation

Den.	The electron density in cm^{-3} (log scale)
Key	A number assigned to each level as given in Table I
Population	The fractional level populations n_j as a function of electron density for an electron temperature log T_e(K)=5.0: the sum of all fractional level populations is defined as unity

Table IVA. Ne III Line Intensities: Without Proton Excitation
Table IVB. Ne III Line Intensities: With Proton Excitation

Den.	The electron density in cm^{-3} (log scale)
j and i	The upper and lower levels, where the numbers refer to the Key listed in Table I
Wavelength	The wavelengths in units of Å
Intensity	The relative intensity ($n_j A_{ji}$ in units of photon/sec) for the indicated density given in the table heading and for an electron temperature of log T_e(K)=5.0

Table A. Solar Active Region Intensities from SERTS-89

Wavelength(Å)	Int[erg/cm^2/s/sr]	Transition
283.149	27.4±13.0	$2p^3 3s\ ^3D_{2,3} \rightarrow 2p^4\ ^3P_2$
322.696	20.3±7.9	$2p^3 3s\ ^5S_2 \rightarrow 2p^4\ ^3P_2$
379.306	7.6±2.2	$2s2p^5\ ^1P_1 \rightarrow 2p^4\ ^1D_2$
427.843	3.9±1.8	$2s2p^5\ ^1P_1 \rightarrow 2p^4\ ^1S_0$

Table B. Laboratory EUV Source Intensity Ratios

Lines in Ratio	Measured Ratio	Calculated Ratio	
		$10^{8} cm^{-3}$	$10^{14} cm^{-3}$
282.49Å/(283.15+.17Å)	0.38±0.04	0.036	0.088
(283.65+.66Å)/(283.15+.17Å)	0.50± 0.04	0.50	0.58
283.87Å/(283.15+.17Å)	0.16± 0.04	0.14	0.18
308.56A/313.04Å	0.65±0.05	0.14	0.30
313.68Å/313.04Å	0.56±0.06	0.59	0.59
313.95Å/313.04Å	0.21±0.05	0.20	0.20

Table C. Laboratory Measurements of Ne III Wavelengths

Kelly [41]	Brosius et al. [40]
267.07	267.0256±0.0018
267.53	267.4884±0.0019
267.71	267.6870±0.0025
282.49	282.4948±0.0022
283.15±0.17	283.1745±0.0014
283.66	283.6651±0.0015
283.87	283.8710±0.0047
301.12	301.1242±0.0013
308.56	308.5720±0.0014
313.05	313.0574±0.0014
313.68	313.6919±0.0019
313.92	313.9635±0.0039
379.31	379.3059±0.0013
427.84	427.8521±0.0018

Table I. Calculated and Experimental Energy Levels for Ne III

Key	Configuration	Level	Calculated	Experimental
1	$2s^22p^4$	$^3P_2$	0.	0.
2		$^3P_1$	744.	643.
3		$^3P_0$	1069.	920.
4		$^1D_2$	29219.	25841.
5		$^1S_0$	72484.	55751.
6	$2s2p^5$	$^3P_2$	215348.	204292.
7		$^3P_1$	216008.	204879.
8		$^3P_0$	216367.	205204
9	$2s^22p^33s$	$^5S_2$	291208.	309924.
10		$^3S_1$	302615.	319444.
11		$^1P_1$	315511.	289479.
12		$^3D_3$	337183.	353148.
13		$^3D_2$	337220.	353177.
14		$^3D_1$	337244.	353197.
15		$^1D_2$	342902.	357930.
16		$^3P_2$	366247.	374434.
17		$^3P_1$	366251.	374461.
18		$^3P_0$	366256.	374478.
19		$^1P_1$	372536.	379834.
20	$2s^22p^33d$	$^5D_3$	375214.	394725.
21		$^5D_4$	375214.	394723.
22		$^5D_2$	375215.	394728.
23		$^5D_1$	375216.	394732.
24		$^5D_0$	375217.	
25		$^3D_1$	379666.	398193.
26		$^3D_2$	379672.	398197.
27		$^3D_3$	379687.	398211.
28		$^3F_4$	418461.	435621.
29		$^1S_0$	418472..	
30		$^3F_3$	418480.	435568.
31		$^3F_4$	418507.	435620.
32		$^3G_5$	419115.	436561.
33		$^3G_4$	419145.	436588.
34		$^3G_3$	419169.	436612.
35		$^1G_4$	419585.	
36		$^3D_3$	420119.	436844.
37		$^3D_2$	420166.	436914.
38		$^3D_1$	420195.	436959.
39		$^3S_1$	422761.	444628.
40		$^3P_2$	423128.	444373.
41		$^1P_1$	423187.	439000.

Table I. Calculated and Experimental Energy Levels for Ni XXI

Key	Configuration	Level	Calculated	Experimental
42		$^3P_1$	423254.	444400.
43		$^1D_2$	423286.	440000.
44		$^1P_1$	423377.	439000.
45		$^1F_3$	424816.	442000.
46		$^3F_4$	447943.	
47		$^3F_3$	447995.	
48		$^3F_2$	448034.	
49		$^3P_0$	448748.	457800.
50		$^3P_1$	448782.	457800.
51		$^3P_2$	448852.	457800.
52		$^1D_2$	449213.	458000.
53		$^3D_1$	449762.	460000.
54		$^3D_2$	449781.	460000.
55		$^3D_3$	449783.	460000.
56		$^1F_3$	451070.	460000.
57		$^1P_1$	454855.	459200.

Table II. Ne III Oscillator Strengths, Radiative Decay Rates and Collision Strengths

Low. Lev.	Upp. Lev.	Osc. Str.	Rad. Dec. Rate	Collision Strength Impact Electron Energy (Ry)				
i	j	gf	(1/s)	5	15	25	35	45
1	2		9.253-03	5.182-01	2.995-01	2.561-01	2.430-01	2.375-01
	3		3.505-08	1.202-01	9.551-02	9.502-02	9.656-02	9.760-02
	4		2.581-01	5.308-01	1.641-01	7.505-02	4.236-02	2.701-02
	5		1.715-02	8.738-02	2.241-02	8.654-03	4.252-03	2.414-03
	6	9.102-01	5.631+09	4.073+00	6.150+00	7.234+00	7.958+00	8.498+00
	7	3.045-01	3.159+09	1.367+00	2.054+00	2.414+00	2.655+00	2.835+00
	8			2.041-02	7.310-03	3.758-03	2.334-03	1.624-03
	9	3.674-06	4.156+04	4.251-02	6.960-03	3.079-03	1.718-03	1.092-03
	10	1.826-01	3.717+09	1.444-01	3.747-01	5.047-01	5.925-01	6.584-01
	11	2.532-04	5.603+06	1.221-01	4.092-02	2.035-02	1.235-02	8.476-03
	12	2.281-01	2.471+09	1.377-01	3.699-01	5.109-01	6.072-01	6.802-01
	13	4.310-02	6.539+08	3.425-02	7.078-02	9.661-02	1.145-01	1.281-01
	14	2.946-03	7.450+07	5.331-03	5.289-03	6.791-03	7.905-03	8.762-03
	15	3.358-04	5.268+06	2.138-02	4.131-03	2.295-03	1.727-03	1.508-03
	16	1.126-01	2.014+09	4.933-02	1.405-01	2.027-01	2.458-01	2.786-01
	17	3.700-02	1.103+09	1.708-02	4.618-02	6.654-02	8.071-02	9.149-02
	18			2.374-03	3.490-04	1.460-04	8.100-05	5.200-05
	19	2.140-07	6.603+03	1.529-02	2.407-03	9.010-04	4.550-04	2.710-04
	20	1.273-06	1.707+04	5.268-02	5.247-03	1.668-03	7.880-04	4.540-04
	21			8.301-02	8.736-03	2.840-03	1.353-03	7.800-04
	22	8.133-06	1.527+05	3.346-02	3.248-03	1.030-03	4.940-04	2.930-04
	23	4.261-06	1.334+05	1.906-02	1.840-03	5.820-04	2.790-04	1.660-04
	24			6.248-03	6.030-04	1.880-04	8.800-05	5.100-05
	25	7.235-03	2.319+08	2.003-02	2.470-02	3.029-02	3.524-02	4.068-02
	26	1.083-01	2.083+09	7.444-02	1.842-01	2.483-01	2.942-01	3.319-01
	27	6.049-01	8.310+09	2.902-01	9.492-01	1.295+00	1.520+00	1.681+00
	28	1.984-05	4.636+05	7.782-03	2.259-03	2.013-03	1.992-03	1.995-03
	29			7.323-03	1.007-03	3.430-04	1.680-04	9.800-05
	30	1.346-04	2.247+06	1.575-02	5.667-03	5.509-03	5.617-03	5.664-03
	31			2.923-02	8.379-03	7.631-03	7.645-03	7.720-03
	32			4.413-02	2.705-02	2.833-02	2.923-02	2.981-02
	33			2.489-02	8.619-03	8.035-03	8.056-03	8.126-03
	34	2.427-06	4.062+04	8.557-03	1.903-03	1.504-03	1.414-03	1.345-03
	35			2.655-02	2.846-03	9.240-04	4.660-04	2.940-04
	36	4.296-01	7.226+09	1.431-01	5.309-01	7.470-01	8.926-01	1.001+00
	37	7.329-02	1.726+09	3.544-02	9.255-02	1.289-01	1.543-01	1.740-01
	38	4.696-03	1.843+08	7.353-03	7.193-03	9.369-03	1.114-02	1.275-02
	39	2.642-01	1.050+10	9.127-02	3.381-01	4.768-01	5.710-01	6.420-01
	40	4.923-01	1.176+10	1.815-01	6.755-01	9.389-01	1.116+00	1.249+00
	41	1.195-01	4.756+09	4.637-02	1.588-01	2.194-01	2.601-01	2.907-01
	42			3.417-03	4.670-04	2.080-04	1.330-04	9.900-05
	43	1.548-02	3.701+08	2.688-02	3.237-03	1.265-03	8.070-04	6.500-04
	44	1.243-02	4.955+08	1.362-02	1.298-03	5.620-04	4.120-04	3.660-04
	45	7.762-04	1.335+07	2.249-02	2.769-03	1.861-03	1.853-03	1.971-03
	46			2.478-02	9.070-03	8.610-03	8.701-03	8.810-03
	47	2.816-04	5.385+06	1.380-02	6.558-03	6.637-03	6.712-03	6.542-03

Low. Lev.	Upp. Lev.	Osc. Str.	Rad. Dec. Rate	Collision Strength Impact Electron Energy (Ry)				
i	j	gf	(1/s)	5	15	25	35	45
	48	2.470-05	6.615+05	7.257-03	2.635-03	2.449-03	2.470-03	2.529-03
	49			2.942-03	2.520-04	7.600-05	3.800-05	2.400-05
	50	4.676-02	2.094+09	1.850-02	5.388-02	7.606-02	9.125-02	1.027-01
	51	1.400-01	3.763+09	4.303-02	1.576-01	2.237-01	2.687-01	3.027-01
	52	4.891-05	1.317+06	1.841-02	2.426-03	8.700-04	4.860-04	3.420-04
	53	4.898-03	2.203+08	9.350-03	8.485-03	1.059-02	1.186-02	1.251-02
	54	7.407-02	1.999+09	3.340-02	8.306-02	1.165-01	1.389-01	1.549-01
	55	4.277-01	8.245+09	1.081-01	4.541-01	6.521-01	7.888-01	8.947-01
	56	2.553-05	4.950+05	2.009-02	2.044-03	6.320-04	3.160-04	2.170-04
	57	3.761-06	1.730+05	9.500-03	7.770-04	1.990-04	8.100-05	4.200-05
2	3		1.854-03	1.984-01	6.776-02	3.393-02	2.069-02	1.444-02
	4		7.965-02	3.229-01	9.985-02	4.562-02	2.568-02	1.632-02
	5		3.632+00	5.340-02	1.369-02	5.278-03	2.584-03	1.459-03
	6	3.024-01	1.858+09	1.367+00	2.054+00	2.414+00	2.654+00	2.834+00
	7	1.820-01	1.875+09	8.533-01	1.244+00	1.454+00	1.596+00	1.702+00
	8	2.431-01	7.538+09	1.056+00	1.630+00	1.924+00	2.119+00	2.264+00
	9	9.317-07	1.049+04	2.528-02	4.141-03	1.831-03	1.020-03	6.470-04
	10	1.083-01	2.195+09	8.610-02	2.232-01	3.005-01	3.526-01	3.918-01
	11	3.838-07	8.454+03	7.353-02	2.432-02	1.180-02	6.909-03	4.532-03
	12			9.370-03	1.540-03	7.010-04	4.050-04	2.660-04
	13	1.194-01	1.803+09	6.512-02	1.933-01	2.679-01	3.185-01	3.566-01
	14	4.149-02	1.044+09	3.008-02	6.808-02	9.329-02	1.107-01	1.238-01
	15	3.654-06	5.706+04	1.251-02	2.142-03	9.380-04	5.220-04	3.330-04
	16	4.137-02	7.373+08	1.922-02	5.244-02	7.533-02	9.120-02	1.032-01
	17	2.271-02	6.745+08	1.499-02	2.919-02	4.132-02	4.989-02	5.644-02
	18	3.063-02	2.729+09	9.780-03	3.783-02	5.511-02	6.698-02	7.597-02
	19	1.159-06	3.563+04	9.519-03	1.490-03	5.570-04	2.800-04	1.660-04
	20			3.782-02	4.066-03	1.333-03	6.390-04	3.710-04
	21			3.092-02	2.784-03	8.430-04	3.880-04	2.200-04
	22	2.508-07	4.691+03	2.759-02	2.930-03	9.570-04	4.580-04	2.650-04
	23	3.050-06	9.509+04	1.479-02	1.478-03	4.750-04	2.280-04	1.340-04
	24	3.604-06	3.371+05	4.433-03	4.190-04	1.350-04	6.800-05	4.300-05
	25	1.069-01	3.414+09	5.580-02	1.674-01	2.285-01	2.696-01	3.006-01
	26	3.201-01	6.131+09	1.483-01	5.052-01	6.921-01	8.212-01	9.236-01
	27			2.493-02	1.553-02	1.615-02	1.659-02	1.689-02
	28	5.534-05	1.288+06	9.450-03	3.695-03	3.704-03	3.843-03	4.005-03
	29	4.772-05	5.554+06	4.221-03	6.470-04	2.880-04	2.030-04	1.750-04
	30			1.093-02	1.537-03	8.890-04	7.500-04	7.020-04
	31			7.711-03	2.521-03	2.388-03	2.418-03	2.453-03
	32			1.105-02	1.136-03	3.560-04	1.690-04	9.900-05
	33			1.403-02	1.353-02	1.492-02	1.558-02	1.596-02
	34			1.968-02	8.769-03	8.681-03	8.840-03	8.970-03
	35			1.925-02	2.115-03	7.320-04	4.030-04	2.800-04
	36			1.190-02	2.068-03	1.340-03	1.166-03	1.097-03
	37	2.242-01	5.262+09	6.834-02	2.772-01	3.911-01	4.687-01	5.282-01
	38	7.212-02	2.821+09	2.878-02	8.999-02	1.260-01	1.506-01	1.692-01

Table II. Ne III Oscillator Strengths, Radiative Decay Rates, and Collision Strengths

Low. Lev.	Upp. Lev.	Osc. Str.	Rad. Dec. Rate	Collision Strength Impact Electron Energy (Ry)				
i	j	gf	(1/s)	5	15	25	35	45
45	46		3.681-02	8.412-02	1.754-02	5.888-03	2.704-03	1.486-03
	47		3.027-03	6.491-02	1.398-02	4.753-03	2.222-03	1.249-03
	48		6.300-02	4.622-02	1.043-02	3.749-03	1.912-03	1.221-03
	49			8.250-04	1.000-04	3.900-05	2.000-05	1.200-05
	50		1.914-04	2.877-03	1.045-03	8.770-04	8.350-04	8.360-04
	51		1.324-03	4.889-03	1.897-03	1.579-03	1.506-03	1.541-03
	52		1.814-01	3.559-02	3.501-02	3.314-02	3.332-02	3.539-02
	53		1.386-04	5.641-02	1.555-02	5.357-03	2.570-03	1.518-03
	54		1.031-01	9.278-02	2.516-02	8.434-03	3.852-03	2.104-03
	55		1.441-01	1.327-01	3.580-02	1.202-02	5.508-03	3.031-03
	56		4.153-01	3.302-01	5.708-01	6.685-01	7.180-01	7.425-01
	57		2.511+00	2.598-01	4.488-01	5.153-01	5.487-01	5.652-01
46	47			2.928+00	1.727+00	1.641+00	1.651+00	1.740+00
	48			2.461-01	9.384-02	8.954-02	8.962-02	9.284-02
	49			1.531-01	1.199-01	1.267-01	1.305-01	1.351-01
	50			4.881-01	2.535-01	2.501-01	2.523-01	2.589-01
	51		1.527-07	9.952-01	5.187-01	4.712-01	4.638-01	4.796-01
	52		2.633-09	8.081-01	7.526-02	2.990-02	1.635-02	1.066-02
	53			2.448-01	8.434-02	8.197-02	8.227-02	8.528-02
	54		9.150-06	1.029+00	8.177-01	8.061-01	8.140-01	8.487-01
	55		1.229-04	3.638+00	3.496+00	3.437+00	3.497+00	3.710+00
	56		4.721-05	1.385+00	1.250-01	5.348-02	2.972-02	1.895-02
	57			4.940-01	5.063-02	2.019-02	1.066-02	6.523-03
47	48			2.786+00	1.728+00	1.644+00	1.649+00	1.731+00
	49			1.325-01	1.809-02	7.177-03	3.774-03	2.306-03
	50		5.592-08	4.043-01	2.959-01	2.881-01	2.889-01	2.982-01
	51		6.036-07	6.492-01	3.628-01	3.484-01	3.481-01	3.570-01
	52		1.362-04	6.920-01	6.612-02	3.368-02	2.444-02	2.137-02
	53		1.146-05	7.394-01	7.024-01	6.894-01	6.945-01	7.235-01
	54		1.911-05	1.672+00	1.511+00	1.477+00	1.498+00	1.587+00
	55		8.868-05	1.252+00	1.061+00	1.039+00	1.050+00	1.100+00
	56		6.986-06	1.098+00	9.633-02	4.137-02	2.313-02	1.489-02
	57		2.443-06	3.867-01	3.997-02	1.599-02	8.475-03	5.213-03
48	49		5.151-08	1.058-01	8.047-02	7.444-02	7.433-02	7.925-02
	50		2.468-08	2.974-01	1.161-01	9.484-02	9.027-02	9.383-02
	51		4.167-07	3.961-01	2.696-01	2.768-01	2.826-01	2.915-01
	52		4.973-05	5.296-01	7.400-02	5.418-02	4.889-02	4.790-02
	53		9.909-05	1.198+00	1.147+00	1.122+00	1.136+00	1.201+00
	54		1.415-04	9.672-01	9.199-01	8.967-01	9.029-01	9.436-01
	55		1.251-05	3.658-01	1.820-01	1.767-01	1.771-01	1.832-01
	56		5.122-05	8.010-01	7.602-02	3.708-02	2.428-02	1.878-02
	57		8.733-05	2.813-01	3.381-02	1.650-02	1.115-02	8.939-03
49	50			3.112-01	3.394-02	1.377-02	7.596-03	5.017-03
	51			5.014-01	5.232-01	5.196-01	5.287-01	5.604-01
	52			5.932-02	5.070-03	3.795-03	3.476-03	3.386-03
	53		7.038-07	7.573-02	7.352-03	2.516-03	1.198-03	2.759-03

Table II. Ne III Oscillator Strengths, Radiative Decay Rates, and Collision Strengths

Low. Lev. i	Upp. Lev. j	Osc. Str. gf	Rad. Dec. Rate (1/s)	Collision Strength Impact Electron Energy (Ry) 5	15	25	35	45
	54		7.136-07	7.347-01	8.408-01	8.357-01	8.507-01	8.910-01
	55			1.037-01	3.834-03	1.359-03	6.900-04	2.639-03
	56			1.247-01	1.313-02	5.235-03	2.761-03	1.687-03
	57		3.451-04	1.043-01	1.060-02	4.622-03	2.587-03	1.654-03
50	51			1.483+00	1.198+00	1.165+00	1.178+00	1.245+00
	52		7.675-06	1.828-01	7.364-03	2.770-03	1.451-03	1.058-03
	53		1.826-06	1.050+00	1.145+00	1.135+00	1.154+00	1.209+00
	54		2.264-07	4.538-01	2.297-01	2.153-01	2.153-01	2.300-01
	55		6.307-07	1.266+00	1.224+00	1.213+00	1.235+00	1.299+00
	56			3.762-01	3.958-02	1.584-02	8.399-03	5.166-03
	57		2.426-04	3.142-01	3.178-02	1.406-02	8.016-03	5.245-03
51	52		1.360-05	3.462-01	3.875-02	2.933-02	2.690-02	2.659-02
	53		3.377-06	4.999-01	3.908-01	3.850-01	3.910-01	4.131-01
	54		7.348-07	1.547+00	1.501+00	1.487+00	1.513+00	1.591+00
	55		3.046-06	2.621+00	2.517+00	2.482+00	2.525+00	2.656+00
	56		4.304-07	6.434-01	8.358-02	4.412-02	3.202-02	2.748-02
	57		4.724-04	5.363-01	6.764-02	3.880-02	2.929-02	2.527-02
52	53		1.204-04	5.406-01	5.272-02	3.027-02	2.350-02	2.118-02
	54		1.523-05	7.747-01	8.886-02	4.897-02	3.634-02	3.141-02
	55		5.763-05	1.005+00	1.322-01	5.680-02	3.184-02	2.096-02
	56		3.242-05	2.631+00	3.208+00	3.206+00	3.262+00	3.426+00
	57		1.741-02	2.213+00	2.634+00	2.620+00	2.664+00	2.746+00
53	54			1.282+00	7.450-01	6.862-01	6.813-01	7.157-01
	55			3.200-01	2.400-01	2.411-01	2.440-01	2.603-01
	56			4.398-01	3.204-02	1.237-02	6.576-03	4.121-03
	57		3.897-05	1.201-01	4.889-03	1.983-03	1.138-03	7.810-04
54	55			1.717+00	9.500-01	9.052-01	9.045-01	9.494-01
	56		5.640-06	7.664-01	1.142-01	8.203-02	7.364-02	7.268-02
	57		2.043-04	2.420-01	6.200-02	5.698-02	5.650-02	5.756-02
55	56		1.184-05	1.016+00	7.424-02	2.847-02	1.499-02	9.279-03
	57		6.593-07	2.814-01	1.159-02	4.923-03	2.997-03	2.183-03
56	57		2.699-04	4.274-01	6.352-01	6.523-01	6.646-01	6.673-01

TABLE IIIA. Ne III Fractional Level Populations: Without Proton Excitation

log(Den.)	8	9	10	11	12	13	14
Key				Population			
1	4.523-01	4.080-01	4.013-01	4.005-01	4.000-01	3.977-01	3.935-01
2	2.567-01	2.425-01	2.382-01	2.373-01	2.370-01	2.357-01	2.334-01
3	8.074-02	7.927-02	7.872-02	7.860-02	7.852-02	7.810-02	7.735-02
4	2.087-01	2.594-01	2.585-01	2.572-01	2.569-01	2.555-01	2.529-01
5	1.604-03	1.080-02	2.325-02	2.625-02	2.657-02	2.647-02	2.621-02
6	6.474-12	6.017-11	5.949-10	5.941-09	5.934-08	5.899-07	5.834-06
7	3.714-12	3.540-11	3.510-10	3.506-09	3.502-08	3.482-07	3.446-06
8	1.231-12	1.181-11	1.167-10	1.165-09	1.164-08	1.157-07	1.145-06
9	1.680-08	1.551-07	1.525-06	1.516-05	1.460-04	1.117-03	4.013-03
10	7.562-14	7.004-13	6.896-12	6.879-11	6.871-10	6.832-09	6.762-08
11	1.846-13	2.349-12	2.505-11	2.535-10	2.536-09	2.523-08	2.498-07
12	2.039-13	2.182-12	2.162-11	2.150-10	2.109-09	1.876-08	1.567-07
13	1.249-13	1.349-12	1.337-11	1.330-10	1.313-09	1.216-08	1.078-07
14	5.741-14	6.239-13	6.190-12	6.167-11	6.159-10	6.125-09	6.064-08
15	5.668-14	6.328-13	6.288-12	6.258-11	6.191-10	5.822-09	5.337-08
16	3.907-14	4.637-13	5.493-12	5.694-11	5.690-10	5.492-09	5.043-08
17	2.308-14	2.764-13	3.200-12	3.302-11	3.311-10	3.294-09	3.262-08
18	7.598-15	9.170-14	1.062-12	1.096-11	1.099-10	1.093-09	1.082-08
19	1.290-14	1.737-13	2.375-12	2.529-11	2.545-10	2.533-09	2.507-08
20	7.237-09	6.685-08	6.576-07	6.543-06	6.387-05	5.176-04	1.797-03
21	3.331-08	3.062-07	3.011-06	2.979-05	2.749-04	1.553-03	2.890-03
22	7.600-10	7.051-09	6.940-08	6.919-07	6.888-06	6.622-05	4.923-04
23	2.621-10	2.440-09	2.403-08	2.396-07	2.389-06	2.329-05	1.930-04
24	7.222-11	6.736-10	6.637-09	6.619-08	6.601-07	6.458-06	5.503-05
25	1.113-14	1.060-13	1.046-12	1.044-11	1.043-10	1.037-09	1.027-08
26	1.855-14	1.729-13	1.702-12	1.698-11	1.696-10	1.686-09	1.669-08
27	3.031-14	2.763-13	2.721-12	2.716-11	2.712-10	2.697-09	2.669-08
28	2.249-11	2.595-10	2.581-09	2.571-08	2.566-07	2.546-06	2.461-05
29	2.128-12	2.086-11	2.059-10	2.053-09	2.050-08	2.037-07	1.997-06
30	2.500-11	2.876-10	2.857-09	2.845-08	2.840-07	2.819-06	2.739-05
31	1.210-08	1.388-07	1.379-06	1.364-05	1.271-04	7.586-04	1.503-03
32	1.243-08	1.356-07	1.343-06	1.330-05	1.257-04	8.104-04	1.777-03
33	1.004-08	1.101-07	1.092-06	1.081-05	1.022-04	6.602-04	1.452-03
34	1.350-11	1.457-10	1.444-09	1.439-08	1.437-07	1.427-06	1.400-05
35	1.263-08	1.276-07	1.261-06	1.249-05	1.171-04	7.196-04	1.478-03
36	1.562-14	1.608-13	1.592-12	1.587-11	1.585-10	1.576-09	1.560-08
37	1.146-14	1.198-13	1.185-12	1.181-11	1.180-10	1.173-09	1.161-08
38	6.457-15	6.894-14	6.834-13	6.810-12	6.801-11	6.764-10	6.697-09
39	4.148-15	3.954-14	3.898-13	3.887-12	3.882-11	3.861-10	3.821-09
40	8.066-15	7.804-14	7.716-13	7.698-12	7.689-11	7.646-10	7.568-09
41	4.647-15	4.615-14	4.569-13	4.557-12	4.552-11	4.527-10	4.481-09
42	1.543-15	1.537-14	1.519-13	1.515-12	1.513-11	1.504-10	1.489-09
43	6.442-15	7.140-14	7.098-13	7.072-12	7.063-11	7.024-10	6.954-09
44	5.457-15	6.612-14	6.869-13	6.911-12	6.910-11	6.873-10	6.805-09
45	6.981-15	8.174-14	8.136-13	8.102-12	8.091-11	8.047-10	7.967-09
46	2.352-09	2.972-08	3.554-07	3.680-06	3.585-05	2.764-04	8.417-04

TABLE IIIA. Ne III Fractional Level Populations: Without Proton Excitation

log(Den.)	8	9	10	11	12	13	14
Key				Population			
47	1.873-12	2.378-11	2.884-10	3.003-09	3.014-08	2.998-07	2.959-06
48	1.667-12	2.126-11	2.577-10	2.683-09	2.692-08	2.678-07	2.641-06
49	1.065-15	1.315-14	1.646-13	1.726-12	1.734-11	1.725-10	1.708-09
50	3.278-15	4.044-14	5.073-13	5.320-12	5.344-11	5.318-10	5.265-09
51	5.583-15	6.866-14	8.725-13	9.175-12	9.218-11	9.173-10	9.081-09
52	6.477-15	7.075-14	7.418-13	7.493-12	7.495-11	7.455-10	7.380-09
53	2.484-15	2.647-14	2.834-13	2.878-12	2.881-11	2.866-10	2.837-09
54	4.188-15	4.364-14	4.677-13	4.753-12	4.758-11	4.732-10	4.685-09
55	6.123-15	6.272-14	6.737-13	6.852-12	6.859-11	6.822-10	6.753-09
56	4.243-15	4.878-14	5.004-13	5.023-12	5.021-11	4.994-10	4.944-09
57	5.993-16	1.087-14	1.744-13	1.903-12	1.919-11	1.911-10	1.892-09

TABLE IIIB. Ne III Fractional Level Populations: With Proton Excitation

log(Den.)	8	9	10	11	12	13	14
Key				Population			
1	4.291-01	3.874-01	3.810-01	3.802-01	3.798-01	3.776-01	3.737-01
2	2.709-01	2.550-01	2.505-01	2.497-01	2.493-01	2.480-01	2.455-01
3	8.953-02	8.720-02	8.651-02	8.637-02	8.628-02	8.582-02	8.499-02
4	2.089-01	2.596-01	2.587-01	2.574-01	2.570-01	2.556-01	2.531-01
5	1.605-03	1.081-02	2.327-02	2.627-02	2.659-02	2.648-02	2.623-02
6	6.322-12	5.881-11	5.815-10	5.807-09	5.801-08	5.766-07	5.703-06
7	3.803-12	3.620-11	3.589-10	3.584-09	3.580-08	3.560-07	3.524-06
8	1.294-12	1.237-11	1.222-10	1.219-09	1.218-08	1.211-07	1.199-06
9	1.675-08	1.546-07	1.521-06	1.512-05	1.456-04	1.115-03	4.012-03
10	7.560-14	7.002-13	6.893-12	6.876-11	6.868-10	6.830-09	6.760-08
11	1.848-13	2.350-12	2.507-11	2.537-10	2.538-09	2.524-08	2.499-07
12	2.000-13	2.148-12	2.128-11	2.116-10	2.076-09	1.845-08	1.538-07
13	1.259-13	1.358-12	1.346-11	1.339-10	1.322-09	1.225-08	1.087-07
14	5.922-14	6.402-13	6.350-12	6.327-11	6.318-10	6.284-09	6.221-08
15	5.690-14	6.348-13	6.308-12	6.278-11	6.211-10	5.839-09	5.353-08
16	3.866-14	4.601-13	5.458-12	5.659-11	5.655-10	5.459-09	5.011-08
17	2.334-14	2.788-13	3.224-12	3.326-11	3.335-10	3.318-09	3.285-08
18	7.762-15	9.318-14	1.077-12	1.110-11	1.113-10	1.108-09	1.097-08
19	1.292-14	1.739-13	2.378-12	2.532-11	2.547-10	2.535-09	2.510-08
20	7.238-09	6.686-08	6.576-07	6.543-06	6.387-05	5.176-04	1.797-03
21	3.293-08	3.029-07	2.978-06	2.946-05	2.719-04	1.536-03	2.859-03
22	7.665-10	7.109-09	6.996-08	6.976-07	6.944-06	6.676-05	4.963-04
23	2.658-10	2.473-09	2.435-08	2.429-07	2.421-06	2.361-05	1.957-04
24	7.344-11	6.845-10	6.744-09	6.726-08	6.707-07	6.562-06	5.592-05
25	1.171-14	1.111-13	1.097-12	1.094-11	1.093-10	1.087-09	1.076-08
26	1.882-14	1.753-13	1.726-12	1.721-11	1.719-10	1.710-09	1.692-08
27	2.925-14	2.669-13	2.628-12	2.622-11	2.619-10	2.605-09	2.577-08
28	2.267-11	2.612-10	2.597-09	2.586-08	2.582-07	2.562-06	2.477-05
29	2.125-12	2.084-11	2.057-10	2.051-09	2.048-08	2.035-07	1.995-06
30	2.504-11	2.880-10	2.861-09	2.848-08	2.844-07	2.823-06	2.742-05
31	1.201-08	1.381-07	1.372-06	1.356-05	1.264-04	7.545-04	1.494-03
32	1.227-08	1.341-07	1.329-06	1.316-05	1.243-04	8.018-04	1.758-03
33	1.006-08	1.103-07	1.093-06	1.083-05	1.023-04	6.611-04	1.454-03
34	1.378-11	1.482-10	1.469-09	1.464-08	1.462-07	1.452-06	1.424-05
35	1.269-08	1.282-07	1.267-06	1.255-05	1.176-04	7.230-04	1.485-03
36	1.525-14	1.575-13	1.559-12	1.554-11	1.552-10	1.543-09	1.528-08
37	1.162-14	1.212-13	1.199-12	1.194-11	1.193-10	1.186-09	1.174-08
38	6.679-15	7.092-14	7.030-13	7.005-12	6.996-11	6.958-10	6.889-09
39	4.098-15	3.910-14	3.854-13	3.843-12	3.838-11	3.817-10	3.778-09
40	7.907-15	7.662-14	7.577-13	7.559-12	7.550-11	7.508-10	7.431-09
41	4.773-15	4.728-14	4.679-13	4.667-12	4.662-11	4.636-10	4.590-09
42	1.604-15	1.591-14	1.572-13	1.568-12	1.566-11	1.557-10	1.542-09
43	6.446-15	7.144-14	7.101-13	7.076-12	7.067-11	7.028-10	6.958-09
44	5.467-15	6.623-14	6.880-13	6.922-12	6.920-11	6.884-10	6.815-09
45	6.994-15	8.186-14	8.148-13	8.114-12	8.102-11	8.059-10	7.978-09
46	2.337-09	2.959-08	3.541-07	3.667-06	3.572-05	2.754-04	8.388-04

TABLE IIIB. Ne III Fractional Level Populations: With Proton Excitation

log(Den.)	8	9	10	11	12	13	14
Key				Population			
47	1.882-12	2.386-11	2.892-10	3.011-09	3.022-08	3.006-07	2.967-06
48	1.691-12	2.148-11	2.599-10	2.705-09	2.714-08	2.700-07	2.663-06
49	1.090-15	1.337-14	1.669-13	1.748-12	1.756-11	1.747-10	1.730-09
50	3.316-15	4.079-14	5.108-13	5.355-12	5.379-11	5.352-10	5.299-09
51	5.515-15	6.806-14	8.668-13	9.117-12	9.161-11	9.116-10	9.025-09
52	6.511-15	7.105-14	7.447-13	7.522-12	7.524-11	7.484-10	7.410-09
53	2.590-15	2.743-14	2.928-13	2.972-12	2.975-11	2.959-10	2.930-09
54	4.247-15	4.416-14	4.728-13	4.804-12	4.809-11	4.783-10	4.735-09
55	5.954-15	6.122-14	6.590-13	6.705-12	6.712-11	6.676-10	6.609-09
56	4.249-15	4.883-14	5.010-13	5.029-12	5.026-11	5.000-10	4.950-09
57	5.997-16	1.088-14	1.746-13	1.904-12	1.920-11	1.912-10	1.893-09

TABLE IVA. Ne III Line Photon Intensities: Without Proton Excitation

log(Den.)			8	9	10	11	12	13	14
j	i	Wavelength			Intensity (Photons)				
55	1	217.392	5.05-05	5.17-04	5.55-03	5.65-02	5.66-01	5.62+00	5.57+01
54	2	217.696	2.69-05	2.80-04	3.00-03	3.05-02	3.06-01	3.04+00	3.01+01
53	2	217.696	8.94-06	9.53-05	1.02-03	1.04-02	1.04-01	1.03+00	1.02+01
53	3	217.828	1.24-05	1.32-04	1.42-03	1.44-02	1.44-01	1.43+00	1.42+01
50	1	218.436	6.86-06	8.47-05	1.06-03	1.11-02	1.12-01	1.11+00	1.10+01
51	1	218.436	2.10-05	2.58-04	3.28-03	3.45-02	3.47-01	3.45+00	3.42+01
47	1	223.217	1.01-05	1.28-04	1.55-03	1.62-02	1.62-01	1.61+00	1.59+01
39	1	224.907	4.36-05	4.15-04	4.09-03	4.08-02	4.08-01	4.05+00	4.01+01
41	1	225.023	2.21-05	2.20-04	2.17-03	2.17-02	2.16-01	2.15+00	2.13+01
40	1	225.037	9.49-05	9.18-04	9.07-03	9.05-02	9.04-01	8.99+00	8.90+01
39	2	225.233	1.86-05	1.78-04	1.75-03	1.75-02	1.74-01	1.73+00	1.72+01
42	2	225.339	2.39-05	2.38-04	2.35-03	2.34-02	2.34-01	2.33+00	2.30+01
41	2	225.349	1.80-05	1.79-04	1.77-03	1.77-02	1.77-01	1.76+00	1.74+01
40	2	225.363	3.09-05	2.99-04	2.96-03	2.95-02	2.95-01	2.93+00	2.90+01
41	3	225.490	2.16-05	2.15-04	2.12-03	2.12-02	2.12-01	2.10+00	2.08+01
37	1	228.878	1.98-05	2.07-04	2.05-03	2.04-02	2.04-01	2.02+00	2.00+01
36	1	228.915	1.13-04	1.16-03	1.15-02	1.15-01	1.15+00	1.14+01	1.13+02
38	2	229.192	1.82-05	1.94-04	1.93-03	1.92-02	1.92-01	1.91+00	1.89+01
37	2	229.216	6.03-05	6.30-04	6.24-03	6.21-02	6.21-01	6.17+00	6.11+01
38	3	229.338	2.46-05	2.62-04	2.60-03	2.59-02	2.59-01	2.57+00	2.55+01
30	1	229.586	5.62-05	6.46-04	6.42-03	6.39-02	6.38-01	6.34+00	6.15+01
28	1	229.607	1.04-05	1.20-04	1.20-03	1.19-02	1.19-01	1.18+00	1.14+01
28	2	229.946	2.90-05	3.34-04	3.32-03	3.31-02	3.31-01	3.28+00	3.17+01
56	4	230.331	4.26-05	4.90-04	5.03-03	5.05-02	5.05-01	5.02+00	4.97+01
52	4	231.397	2.46-05	2.69-04	2.82-03	2.84-02	2.85-01	2.83+00	2.80+01
48	4	238.769	9.18-06	1.17-04	1.42-03	1.48-02	1.48-01	1.47+00	1.45+01
47	4	238.792	1.06-05	1.34-04	1.63-03	1.69-02	1.70-01	1.69+00	1.67+01
29	2	239.391	1.18-05	1.16-04	1.14-03	1.14-02	1.14-01	1.13+00	1.11+01
45	4	240.293	1.10-04	1.28-03	1.28-02	1.27-01	1.27+00	1.26+01	1.25+02
43	4	241.454	7.73-05	8.57-04	8.52-03	8.49-02	8.48-01	8.43+00	8.34+01
44	4	242.038	5.53-05	6.70-04	6.96-03	7.00-02	7.00-01	6.96+00	6.89+01
34	4	243.445	3.87-05	4.18-04	4.14-03	4.13-02	4.12-01	4.10+00	4.02+01
57	5	247.863	1.06-05	1.92-04	3.07-03	3.35-02	3.38-01	3.37+00	3.33+01
27	1	251.124	2.52-04	2.30-03	2.26-02	2.26-01	2.25+00	2.24+01	2.22+02
26	1	251.133	3.86-05	3.60-04	3.55-03	3.54-02	3.53-01	3.51+00	3.48+01
26	2	251.539	1.14-04	1.06-03	1.04-02	1.04-01	1.04+00	1.03+01	1.02+02
25	2	251.541	3.80-05	3.62-04	3.57-03	3.56-02	3.56-01	3.54+00	3.51+01
25	3	251.717	5.03-05	4.79-04	4.73-03	4.72-02	4.71-01	4.69+00	4.64+01
23	1	253.337	3.50-05	3.25-04	3.21-03	3.20-02	3.19-01	3.11+00	2.58+01
22	1	253.339	1.16-04	1.08-03	1.06-02	1.06-01	1.05+00	1.01+01	7.52+01
20	1	253.340	1.24-04	1.14-03	1.12-02	1.12-01	1.09+00	8.84+00	3.07+01
23	2	253.750	2.49-05	2.32-04	2.28-03	2.28-02	2.27-01	2.21+00	1.84+01
23	3	253.929	1.28-05	1.19-04	1.17-03	1.17-02	1.17-01	1.14+00	9.42+00
24	2	267.042	2.43-05	2.27-04	2.24-03	2.23-02	2.23-01	2.18+00	1.85+01
17	1	267.051	2.55-05	3.05-04	3.53-03	3.64-02	3.65-01	3.63+00	3.60+01

TABLE IVB. Ne III Line Photon Intensities: With Proton Excitation

log(Den.)			8	9	10	11	12	13	14
j	i	Wavelength			Intensity (Photons)				
16	1	267.070	7.79-05	9.27-04	1.10-02	1.14-01	1.14+00	1.10+01	1.01+02
18	2	267.498	2.12-05	2.54-04	2.94-03	3.03-02	3.04-01	3.02+00	2.99+01
17	2	267.510	1.57-05	1.88-04	2.17-03	2.24-02	2.25-01	2.24+00	2.22+01
16	2	267.530	2.85-05	3.39-04	4.02-03	4.17-02	4.17-01	4.02+00	3.69+01
17	3	267.709	2.24-05	2.68-04	3.10-03	3.19-02	3.20-01	3.19+00	3.15+01
19	4	282.492	2.05-05	2.76-04	3.78-03	4.02-02	4.04-01	4.03+00	3.99+01
13	1	283.145	8.23-05	8.88-04	8.80-03	8.75-02	8.65-01	8.01+00	7.11+01
12	1	283.168	4.94-04	5.31-03	5.26-02	5.23-01	5.13+00	4.56+01	3.80+02
14	2	283.645	6.18-05	6.68-04	6.63-03	6.60-02	6.60-01	6.56+00	6.50+01
13	2	283.661	2.27-04	2.45-03	2.43-02	2.41-01	2.38+00	2.21+01	1.96+02
14	3	283.868	7.88-05	8.51-04	8.45-03	8.41-02	8.40-01	8.36+00	8.27+01
15	4	301.125	3.23-04	3.61-03	3.59-02	3.57-01	3.53+00	3.32+01	3.04+02
19	5	308.563	3.92-05	5.28-04	7.22-03	7.69-02	7.74-01	7.70+00	7.63+01
10	1	313.044	2.81-04	2.60-03	2.56-02	2.56-01	2.55+00	2.54+01	2.51+02
10	2	313.675	1.66-04	1.54-03	1.51-02	1.51-01	1.51+00	1.50+01	1.48+02
10	3	313.948	5.50-05	5.10-04	5.02-03	5.00-02	5.00-01	4.97+00	4.92+01
9	1	322.660	6.96-04	6.43-03	6.32-02	6.28-01	6.05+00	4.63+01	1.67+02
9	2	323.331	1.76-04	1.62-03	1.60-02	1.59-01	1.53+00	1.17+01	4.21+01
11	4	379.308	5.62-03	7.14-02	7.62-01	7.71+00	7.71+01	7.67+02	7.60+03
11	5	427.847	4.83-04	6.14-03	6.55-02	6.63-01	6.63+00	6.60+01	6.53+02
46	6	429.933	1.57-05	1.99-04	2.38-03	2.47-02	2.40-01	1.85+00	5.64+00
7	1	488.094	1.20-02	1.14-01	1.13+00	1.13+01	1.13+02	1.12+03	1.11+04
8	2	488.852	9.75-03	9.32-02	9.21-01	9.19+00	9.18+01	9.13+02	9.04+03
6	1	489.496	3.56-02	3.31-01	3.27+00	3.27+01	3.27+02	3.25+03	3.21+04
7	2	489.630	7.13-03	6.79-02	6.73-01	6.72+00	6.71+01	6.68+02	6.61+03
7	3	490.297	9.46-03	9.01-02	8.93-01	8.92+00	8.91+01	8.86+02	8.77+03
6	2	491.042	1.17-02	1.09-01	1.08+00	1.08+01	1.08+02	1.07+03	1.06+04
20	9	1179.198	4.94-05	4.56-04	4.49-03	4.47-02	4.36-01	3.53+00	1.23+01
21	9	1179.260	2.25-04	2.07-03	2.03-02	2.01-01	1.86+00	1.05+01	1.95+01
32	12	1198.852	7.33-05	8.02-04	7.94-03	7.87-02	7.43-01	4.79+00	1.05+01
33	13	1198.882	5.34-05	5.86-04	5.81-03	5.75-02	5.43-01	3.51+00	7.72+00
31	12	1212.524	6.22-05	7.14-04	7.10-03	7.02-02	6.54-01	3.90+00	7.73+00
46	16	1224.052	1.33-05	1.68-04	2.02-03	2.09-02	2.03-01	1.57+00	4.77+00
35	15	1304.072	5.42-05	5.48-04	5.41-03	5.36-02	5.02-01	3.09+00	6.34+00

Figure Caption

Figure 1. Ne III lines recorded during testing of the SERTS rocket instrument after its flight in 1995. The emission was produced by a hollow cathode laboratory source containing Neon gas and operated at high voltage. Positions of lines listed in Table IV of this paper are indicated by tic marks below the spectrum segments.

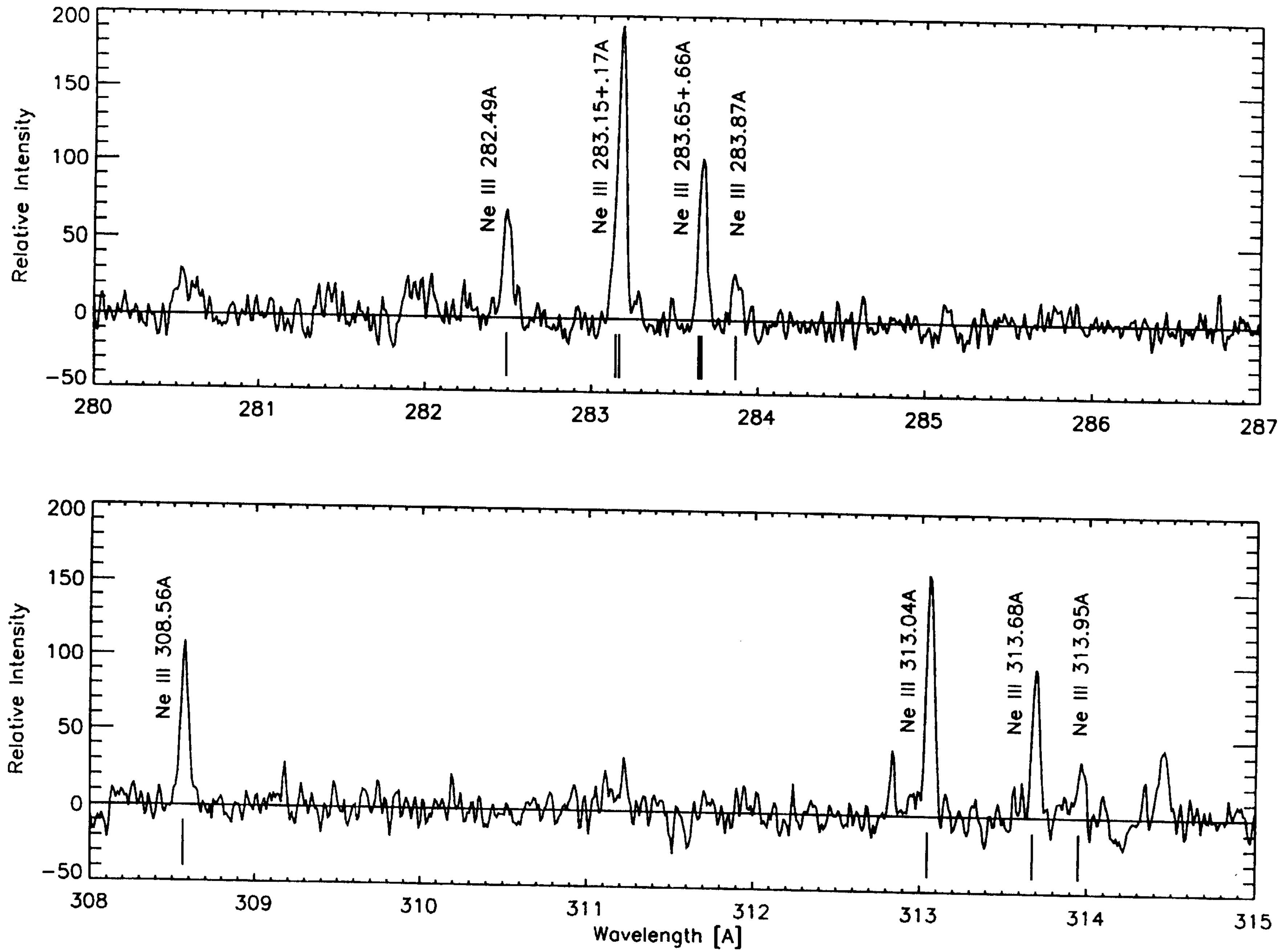
Relative Intensity
200
150
100
50
0
−50
280
281
282
283
284
285
286
287
Ne III 282.49A
Ne III 283.15+.17A
Ne III 283.65+.66A
Ne III 283.87A
Relative Intensity
308
309
310
311
312
313
314
315
Wavelength [A]
Ne III 308.56A
Ne III 313.04A
Ne III 313.68A
Ne III 313.95A